1999

An Iron-Based Ecosystem Model of the Central Equatorial Pacific

Carrie L. Leonard

Charles R. McClain

Ragu Murtugudde

Eileen E. Hofmann
Old Dominion University, ehofmann@odu.edu

Lawrence W. Harding Jr.

Original Publication Citation

Leonard, C.L., McClain, C.R., Murtugudde, R., Hofmann, E.E., & Harding, L.W. (1999). An iron-based ecosystem model of the central equatorial Pacific. *Journal of Geophysical Research-Oceans, 104*(C1), 1325-1341. doi: 10.1029/1998jc900049

JOURNAL OF GEOPHYSICAL RESEARCH, VOL. 104, NO. C1, PAGES 1325–1341, JANUARY 15, 1999

An iron-based ecosystem model of the central equatorial Pacific

Carrie L. Leonard,[1,2] Charles R. McClain,[3] Ragu Murtugudde,[4] Eileen E. Hofmann,[5] and Lawrence W. Harding Jr.[6,7]

Abstract. The central and eastern equatorial Pacific region is characterized by lower than expected phytoplankton biomass and primary production given the relatively high ambient nitrate concentrations. These unusual conditions have spawned several field programs and laboratory experiments to determine why this high nitrate–low chlorophyll pattern persists in this region. To synthesize the results from these field programs, as well as providing additional evidence in support of the iron hypothesis, we developed a one-dimensional, nine-component ecosystem model of 0°N 140°W. The model components include two phytoplankton size fractions, two zooplankton size fractions, two detrital size fractions, dissolved iron, nitrate, and ammonium. The model was run for 5 years (1990–1994) and was forced using an atmospheric radiative transfer model, an ocean general circulation model (GCM), and in situ data. To our knowledge, this is the first ecosystem model at 0°N 140°W to synthesize the Joint Global Ocean Flux Study Equatorial Pacific Process Study (JGOFS EqPac) data set, as well as to use both in situ and modeled physical data to drive the model. Modeled phytoplankton, zooplankton, and iron all varied on interannual timescales due to El Niño events. Total phytoplankton biomass increased by as much as 40% from early 1992 (El Niño warm) to 1993 (normal). The results also indicate that the biomass increase during a cool period is not constant for each phytoplankton component, but instead the increase is most evident in the netphytoplankton (>10 μm). Netphytoplankton increase from a low of 0.1% of the total chlorophyll in 1992 to a high of 30% of the total in 1993. Microzooplankton grazing rates fluctuated in response to changes in nanophytoplankton growth rates, whereas mesozooplankton grazing was unrelated to netphytoplankton growth rates. The magnitude and temporal variability of phytoplankton chlorophyll agreed well with in situ data collected during 1992. Modeled primary production was lower than measured during El Niño but agreed with observations during normal conditions. The low primary productivity was probably a result of downwelling produced by the physical model. New production was calculated from total and recycled iron rather than nitrate-based production and was more variable in general and almost 3 times the nitrate-based new production during non-El Niño conditions.

1. Introduction

The central and eastern equatorial Pacific is characterized by a tongue of cool, macronutrient-rich water, especially compared to the areas just north and south of the region. The cold tongue supports a region of consistently elevated phytoplankton biomass and productivity [*Berger*, 1989]. This feature, supported by Ekman divergence and upwelling along the equator, shows little seasonality yet can be dramatically affected by interannual El Niño events. These large-scale physical events, which reduce the flux of cold water to the ocean surface and the flux of nutrients to the euphotic zone, can cause a 50% reduction in phytoplankton biomass [*Barber and Chavez*, 1986; *Leonard and McClain*, 1996]. Along with the large interannual variations in phytoplankton biomass that characterize the region, the equatorial Pacific is also one of the high nitrate–low chlorophyll (HNLC) regions of the world's oceans. The intriguing questions surrounding the dual phenomena of El Niño and HNLC conditions, combined with the Pacific's size and its possible contribution to global new production, have stimulated a variety of laboratory [e.g., *Martin et al.*, 1991] and in situ investigations (e.g., Joint Global Ocean Flux Study Equatorial Pacific Process Study (JGOFS EqPac): *Murray et al.* [1994]; IRONEX 1 and 2: *Martin et al.* [1994]; *Coale et al.* [1996b]; *Landry et al.* [1997]).

Open ocean ecosystems are often characterized by an inverse relationship between phytoplankton biomass and nitrate concentrations with depth. Nitrate limits both phytoplankton biomass and primary productivity in these regions, with euphotic zone nitrate concentrations approaching zero. This is not the case in the central equatorial Pacific where surface nitrate concentrations are >4 μM, greatly exceeding the

[1]Marine Estuarine Environmental Science Program, University of Maryland, College Park.
[2]Now at Joint Institute for Marine and Atmospheric Research, University of Hawaii, Honolulu.
[3]SeaWiFS Project Office, NASA Goddard Space Flight Center, Greenbelt, Maryland.
[4]Joint Center for Earth Systems Science, University of Maryland, College Park.
[5]Center for Coastal Physical Oceanography, Old Dominion University, Norfolk, Virginia.
[6]Horn Point Laboratory, University of Maryland Center for Environmental Science, Cambridge.
[7]Also at Maryland Sea Grant College, University of Maryland, College Park.

Paper number 1998JC900049.
0148-0227/99/1998JC900049$09.00

amount of nitrogen needed for phytoplankton growth. Recently, the inverse relationship between phytoplankton biomass (as expressed in chlorophyll concentration) and dissolved iron in this region has been offered as an explanation for the area's HNLC conditions [*Martin et al.*, 1991; *Coale et al.*, 1996a]. Iron addition experiments both in the laboratory and in situ have shown higher phytoplankton community growth rates and chlorophyll accumulation in iron-amended samples from the equatorial Pacific [*Martin et al.*, 1991, 1994; *Coale et al.*, 1996b]. In situ growth rates for nanophytoplankton in the region are relatively high, even with the low ambient iron concentrations [*Verity et al.*, 1996; *Landry et al.*, 1995]. The phytoplankton of the central equatorial Pacific Ocean, like most open ocean regions, are dominated by picophytoplankton and nanophytoplankton. Yet most of the additional phytoplankton chlorophyll in the iron-enrichment experiments was due to diatom growth [*Martin et al.*, 1991; *Fitzwater et al.*, 1996]. It appears that nanophytoplankton growth in the central equatorial Pacific can be relatively high since they may be adapted to low iron conditions with lower C:Fe ratios and half-saturation constants for iron uptake, whereas netphytoplankton growth rates are low due to higher molar ratios and higher half-saturation constants [*Price et al.*, 1994; *Sunda and Huntsman*, 1995].

Why are chlorophyll concentrations lower than expected in the equatorial Pacific if nanophytoplankton growth rates are relatively high? Microzooplankton grazing can remove up to 100% of the nanophytoplankton growth each day [*Verity et al.*, 1996]. Microzooplankton grazing also responds quickly to changes in nanophytoplankton growth rates [*Landry et al.*, 1995], so any biomass that may accumulate is quickly removed from the euphotic zone. Therefore, while nanophytoplankton growth is not as subject to marked bottom-up control via nutrient limitation, it is regulated by top-down control due to grazing pressure. Netphytoplankton, on the other hand, are not as strongly grazed because of the lag time between netphytoplankton growth and mesozooplankton grazing [*Dam et al.*, 1995; *Roman and Gauzens*, 1997], but their growth rate is limited by iron supply. Therefore the central equatorial Pacific is a HNLC region with iron supply and microzooplankton grazing working in concert to limit total phytoplankton growth and biomass.

This hypothesis remains difficult to synthesize into one cohesive picture from the individual experiments because of the short temporal nature of field programs and the inherent difficulties of applying results from laboratory experiments to natural systems. The JGOFS EqPac program fortuitously sampled both El Niño and "normal" conditions in the central equatorial Pacific, but the ship sampling portion of the program was still only on the equator for a total of 4 weeks in a region clearly dominated by interannual variability. To aid in the synthesis of the equatorial Pacific data and to provide a time series of phytoplankton, zooplankton, and nutrient concentrations, we have developed a one-dimensional ecosystem model for 0°N 140°W, which is forced with both in situ and modeled physical data for a 5-year period. This model is the first that we know of to model the El Niño and normal phases of the JGOFS EqPac program and to use both in situ and modeled physical forcing to drive the ecosystem. There are prior models of the ecosystem at this site, but they are lacking one or more of the components included here. *Chai et al.* [1996] used realistic physics to drive a basin-scale ecosystem model, but their model did not include iron, which is a critical component influencing the ecosystem. A recent model that does include iron, presented by *Loukos et al.* [1997], uses idealized forcing and does not simulate an El Niño. The Loukos et al. model also contains a simpler ecosystem than the model presented here. Our model contains the majority of the factors that may limit primary production and phytoplankton biomass in the central Pacific (to the first order).

Here we present the results of a one-dimensional, nine-component (two phytoplankton, two zooplankton, two detrital size fractions, iron, ammonium, and nitrate) ecosystem model. Physical oceanographic inputs to the model were supplied from a basin-scale ocean general circulation model (GCM) [*Murtugudde and Busalacchi*, 1998], an atmospheric irradiance model [*Gregg and Carder*, 1990], and in situ data. The following section presents the models used in this study and gives a detailed description of the ecosystem model equations. The next section describes the model output and discuss the results in the context of field programs in the equatorial Pacific. It also gives an analysis of the sensitivity of the model to variations in many of the ecosystem parameters. The final section summarizes and concludes this chapter.

2. Model Description

The one-dimensional (vertical) time-dependent ecosystem model was composed of a set of nine partial differential equations. The model was physically forced using vertical advection and diffusion as well as surface photosynthetically available radiation (PAR). The general form of each equation is

$$\frac{\delta B_i}{\delta t} + (w + w_{bio})\frac{\delta B_i}{\delta z} - \frac{\delta}{\delta z}\left(K_z \frac{\delta B_i}{\delta z}\right) = S_i \qquad i = 1, 9 \qquad (1)$$

where B_i is one of the nine nonconservative components of the ecosystem model (i = (1) nanophytoplankton, (2) netphytoplankton, (3) microzooplankton, (4) mesozooplankton, (5) small detritus, (6) large detritus, (7) nitrate, (8) ammonium, (9) dissolved iron). S_i represents the biological sources and sinks of B_i, w is the vertical advection, w_{bio} is the sinking or migration rate of B_i and K_z is the vertical diffusivity. Explicit descriptions of each S_i are provide in subsequent parts of section 2. The model domain was 120 m in the vertical with 1-m resolution. The model was run for 5 years (1990–1994) with a 1-hour time step using the Crank-Nicholson numerical scheme. These particular 5 years were chosen for two reasons. First, the JGOFS EqPac Program was conducted in 1992, and the data were extensively used for ecosystem parameters and model validation, so the interannual simulation needed to span the program. Second, one of the objectives of this research was to document interannual changes in the ecosystem due to El Niño events so the simulation required both El Niño and normal conditions. Both of these conditions were present at 0°N 140°W during the 1990–1994 time period.

2.1. Vertical Velocity and Diffusion

The w_{bio} was the unique sinking rate for each phytoplankton size fraction and the microzooplankton and also parameterized mesozooplankton vertical migration. The mesozooplankton migration was a cosine function with upward swimming from 1800 to 2400 hours and downward swimming from 0600 to 1100 hours. K_z, the vertical diffusivity coefficient, was a function of vertical temperature and current shear and was calculated using the method of *Pacanowski and Philander* [1981]

from in situ observations retrieved from the Tropical Ocean-Global Atmosphere Tropical Atmosphere-Ocean (TOGA TAO) buoy at 0°N 140°W. In situ observations were used for K_z rather than the physical model output because the physical model poorly reproduced north/south currents due to errors in the wind fields.

Vertical advection w was supplied from an ocean GCM of the tropical Pacific [*Murtugudde and Busalacchi*, 1998]. The ocean GCM was the reduced gravity, primitive equation, sigma coordinate model of *Gent and Cane* [1990] with an embedded hybrid mixed layer model of *Chen et al.* [1994]. Complete hydrology had been added to the model with subsequent improvements in tropical sea surface temperature (SST) and upper ocean hydrology as reported by *Murtugudde et al.* [1996] and *Murtugudde and Busalacchi* [1998]. Vertically, the model consisted of a mixed layer and a prescribed number of layers beneath it, according to a sigma coordinate (10 layers were used for this simulation). Output from the sigma layers was linearly interpolated to give the velocity at 1-m resolution for use with the ecosystem model. The horizontal grid had $\frac{1}{3}°$ resolution near the equator and at the eastern and western boundaries. The model domain spanned the entire Pacific zonally and had meridional boundaries of ±30° latitude. The model was spun up with climatological winds for 10 years. The interannual simulation (1990–1995) was initialized with the climatological run and then forced with monthly mean Florida State University winds.

2.2. Surface Irradiance

Surface photosynthetically available radiation (PAR: 350–700 nm) was calculated using a spectral atmospheric model of marine atmospheres [*Gregg and Carder*, 1990]. Model runs showed little difference in the underwater light distribution between spectral and broadband light fields [cf. *Behrenfeld and Falkowski*, 1997], so a sum of the spectral values from 350 to 700 nm was used to represent surface PAR. Since the irradiance model assumed a cloud-free atmosphere, a simple correction scheme was devised to account for local cloud cover

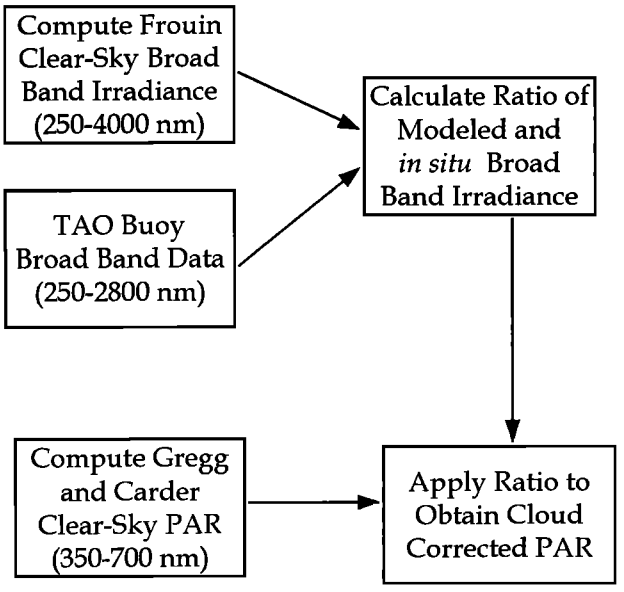

Figure 1. Scheme to correct modeled cloud-free photosynthetically active radiation for cloud cover.

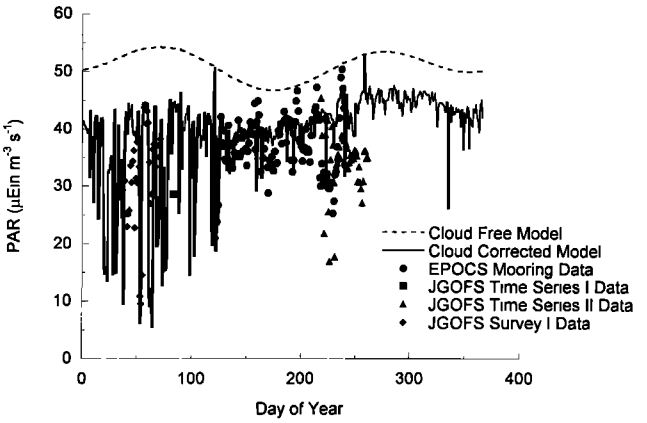

Figure 2. Noontime modeled cloud-free and cloud-corrected surface PAR and averaged daylight in situ PAR at 0°N 140°W for 1992. Cloud-free model (dotted line); cloud-corrected model (solid line); EPOCS mooring data (circles); JGOFS EqPac time series I data (squares); JGOFS EqPac time series II data (triangles); JGOFS EqPac survey I data (diamonds).

[*Tai and McClain*, 1996]. The scheme used a ratio of the broadband irradiance from the TAO buoy at 0°N 140°W to the irradiance calculated using *Frouin et al.*'s [1989] broad band irradiance model. The modeled PAR was then multiplied by the ratio (Figure 1) to obtain cloud-corrected PAR.

The modeled, cloud-corrected surface PAR compared well with in situ PAR data from 1992 (Figure 2), especially early in the year. There are several possible reasons for the discrepancies between the model and the in situ data during the latter part of 1992, when the r^2 fell to 0.3 between the model and the data. First, PAR can be defined as either 350–700 nm or 400–700 nm, and if the latter was used as the in situ definition, the values would be ~7% lower than the modeled PAR. Also, errors such as instrument shading and biofouling can be significant when measuring PAR. Finally, we have compared model output to two different field programs using their own measurement techniques, and the differences in the instruments could be enough to cause the discrepancies between the model output and the data. Even with the less than perfect fit, the cloud-corrected PAR was still a better representation of the in situ data than the clear-sky model, which if used would have led to the overestimation of surface PAR and possibly the primary productivity rates.

2.3. In Situ Data

Data from JGOFS EqPac were used for some of the ecosystem model parameters as well as for model validation. These data can be found at http://www1.whoi.edu/jgofs.html. Physical oceanographic in situ data were required for calculating surface PAR, vertical eddy diffusivity, maximum phytoplankton growth rates and bottom boundary conditions for nutrients. All in situ data were retrieved from the TOGA TAO buoy at 0°N 140°W. These data included hourly relative humidity, wind velocity, air and sea surface temperature (SST), and daily subsurface current and temperature profiles (Table 1). Missing data were replaced with monthly climatological data for each variable (Comprehensive Ocean-Atmosphere Data Set (COADS) winds and relative humidity, Kessler temperature, and Reynolds SST). The profile data were linearly interpolated from the buoy sensor depths to 1 meter resolution for

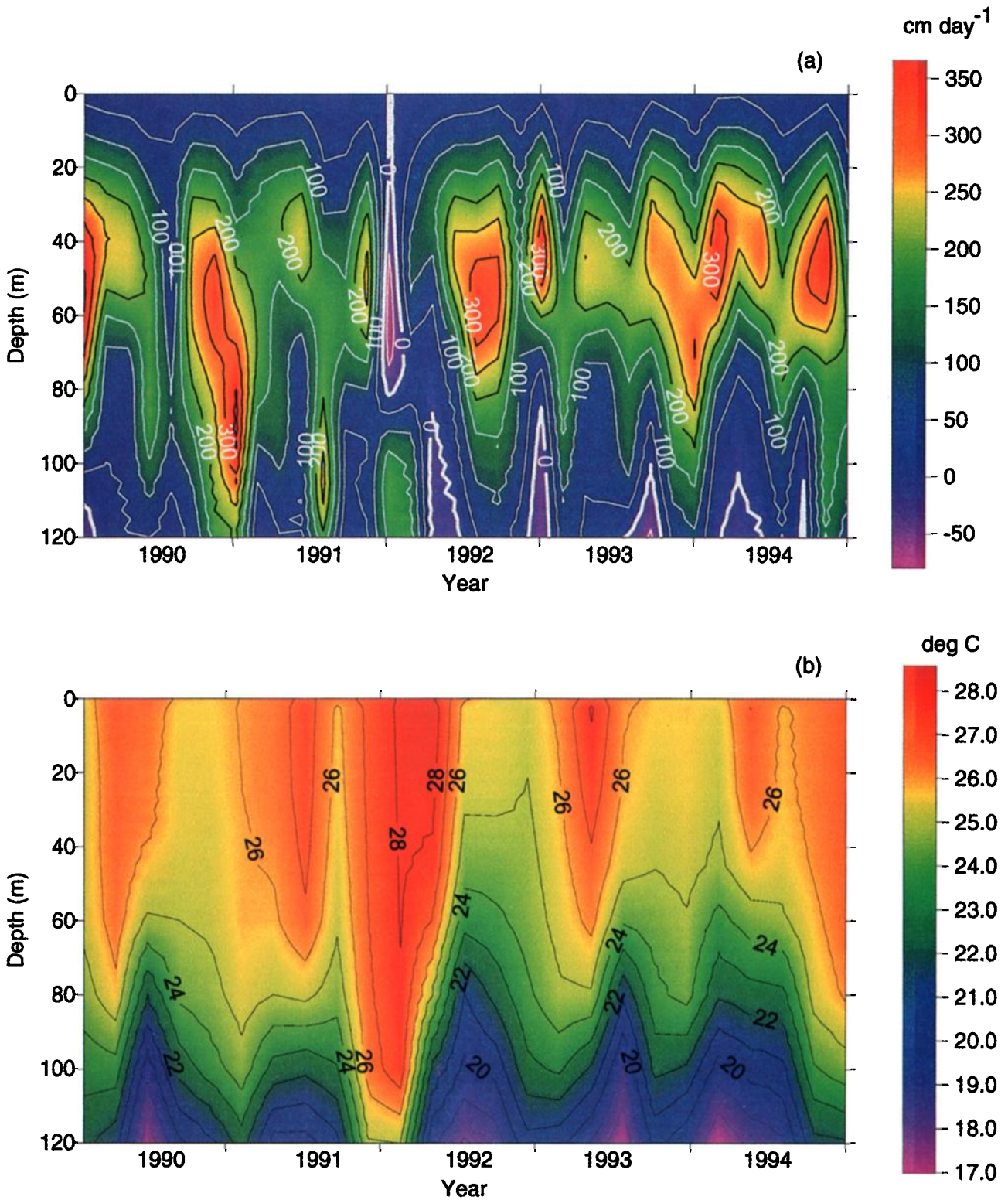

Plate 1. (a) The 1990–1994 10-day vertical advection (cm d^{-1}) from the ocean general circulation model. Contour intervals are 50 cm d^{-1}, and the thick line is the 0 cm d^{-1} contour. (b) Average monthly subsurface temperature from the 0°N 140°W TOGA TAO buoy.

inclusion in the ecosystem model. The data were supplied by the TOGA TAO project at http://www.pmel.noaa.gov/toga-tao/.

2.4. Ecosystem Model

The ecosystem model contains two phytoplankton size fractions, two zooplankton size fractions, dissolved iron, nitrate, ammonium, and two detrital size fractions (Figure 3). Exchanges between the components occur with phytoplankton uptake of nutrients, differential zooplankton grazing, and nutrient recycling. Dissolved iron concentration was calculated in nmol Fe m^{-3}, all other components were in mmol N m^{-3}. The definitions and values of model parameters are listed in Table 2.

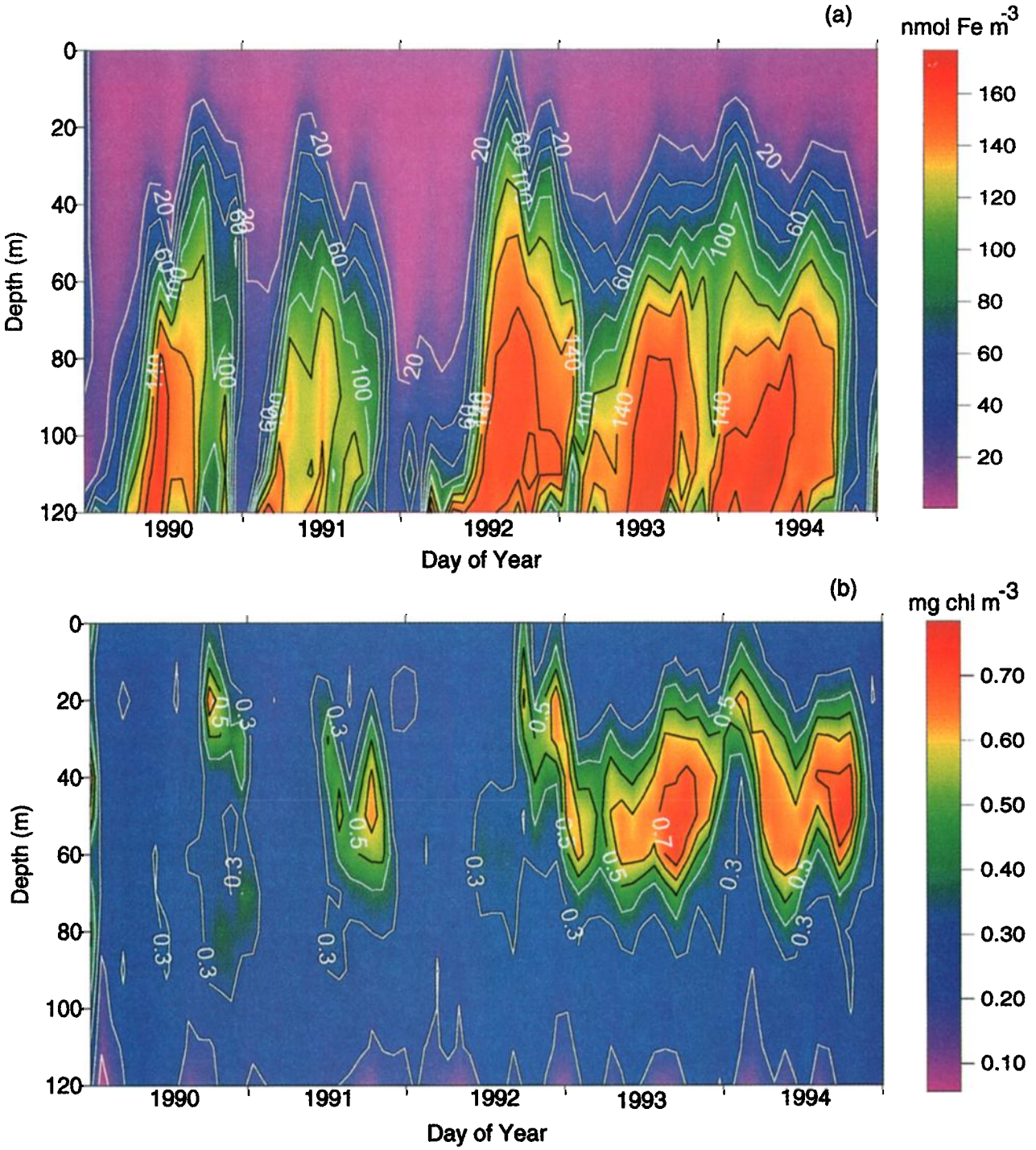

Plate 2. Modeled profiles of (a) iron and (b) phytoplankton from 1990 to 1994. Iron contour intervals are 20 mmol Fe m^{-3}, and phytoplankton contour intervals are 0.1 mg chl m^{-3}.

2.4.1. Phytoplankton. Two phytoplankton size fractions are included in the model: nanophytoplankton (<10 μm) and netphytoplankton (>10 μm). The 10-μm cutoff was used to simply discriminate between diatom and smaller than diatom phytoplankton. Nanophytoplankton P_s dominate the phytoplankton of the equatorial Pacific and are better adapted for growth in low iron concentrations [*Sunda et al.*, 1991; *Sunda and Huntsman*, 1995]. Netphytoplankton P_l, in contrast, require more iron for production, and are found only in substantial numbers during non-El Niño conditions [*Iriarte and Fryxell*, 1995; *Sunda and Huntsman*, 1995]. The growth rate of both size fractions was dependent upon light and nutrient (iron, nitrogen, and ammonium) supply with biomass losses due to zooplankton grazing and mortality.

The change in phytoplankton over time was calculated using

$$S_1 = GL_{\text{lim}}N_{\text{lim}\,s}P_s - g_s\Lambda P_s(1 - e^{-\Lambda P_s})Z_s - \varepsilon_s P_s \quad (2)$$

$$S_2 = GL_{\text{lim}}N_{\text{lim}\,l}P_l - g_l\Lambda P_l(1 - e^{-\Lambda P_l})Z_l - \varepsilon_l P_l \quad (3)$$

Table 1. The 0°N 140°W TOGA TAO Buoy Data Used to Force the Ecosystem Model

Data Type	Resolution	Availability
u and v winds, m s^{-1}	hourly	April 30, 1990, to Oct. 9, 1995
SST, °C	hourly	April 30, 1990, to Oct. 9, 1995
Air temperature, °C	hourly	April 30, 1990, to Oct. 9, 1995
Relative humidity, %	hourly	April 30, 1990, to Oct. 9, 1995
Irradiance, 285–2800 nm	hourly	Nov. 9, 1991, to Sept. 10, 1995
u and v currents, cm s^{-1}	daily	April 16, 1983, to Sept. 9, 1995
Subsurface temperature, °C	daily	Jan. 1, 1990, to Oct. 9, 1995

The terms on the right side of (2) and (3) represent phytoplankton growth G, grazing losses g, and mortality ε. Maximum phytoplankton growth G was computed as a function of temperature calculated using *Eppley*'s [1972] formula:

$$G = G_0 e^{bT} \tag{4}$$

where G_0 is the phytoplankton specific growth rate at 0°C and b is a constant that relates the change in G to the change in temperature at a given depth. The values of G_0 and b were determined from measurements made for a wide range of phytoplankton species and temperatures. The model was not very sensitive to the maximum growth rate formulation since the output did not change when a constant or diurnal-varying growth rate was used (data not shown).

Light limitation was a time- and depth-varying function with α the slope of the photosynthesis-light curve, $P^B_{\max}$ the maximum photosynthetic rate, normalized to biomass, and $I(z, t)$ representing PAR at a given depth and time:

$$L_{\lim} = \left[1 - \exp\left(-\frac{\alpha(z, t)I(z, t)}{P^B_{\max}(z, t)}\right)\right] \tag{5}$$

α and $P^B_{\max}$ were linearly interpolated in both space and time to the model grid from in situ measurements taken at discrete depths and times over a 24 hour period on two independent cruises [*Cullen et al.*, 1992; *Lindley et al.*, 1995]. Each phytoplankton size fraction has the same photosynthetic parameters (Table 2) because neither of the above data sets had sorted the P-I curves by phytoplankton species or size, and we wanted the parameters to reflect the local populations as much as possible. Subsurface PAR was a function of both the depth in the water column z (equation (6)) and the amount of chlorophyll at each depth (equation (7)):

$$I(z) = I(z - \Delta z)e^{-K_d(z)\Delta z} \tag{6}$$

where $K_d(z)$ is the downwelling attenuation coefficient. In this simulation, K_d was calculated for PAR only and is a function of the attenuation due to water and the chlorophyll concentration at each depth

$$K_d(z) = K_w + 0.0321chl(z)^{0.401} \tag{7}$$

The coefficients in (7) were modified from the original *Morel* [1988] formulation for case 1 waters, as the original coefficients produced a shallower than observed euphotic zone.

Phytoplankton nutrient uptake was a function of the concentrations of iron, nitrate, and ammonium at a given depth and time and was based on Michaelis-Menten kinetics and the Monod equation. In addition, ammonium inhibition of nitrate uptake was included as an exponential function of the ammonium concentration [*Price et al.*, 1994].

$$N_{\lim} = \min\left[\frac{N}{k_N + N}e^{-\Psi A} + \frac{A}{k_A + A}, \frac{Fe}{k_{Fe} + Fe}\right] \tag{8}$$

The half saturation constants k_i for each nutrient were specific to each phytoplankton size fraction, resulting in two nutrient limitation parameters, $N_{\lim s}$ and $N_{\lim l}$ (Table 2).

2.4.2. Zooplankton. The zooplankton were split into two size fractions, microzooplankton Z_s and mesozooplankton Z_l. The microzooplankton grazed the nanophytoplankton and the mesozooplankton grazed on netphytoplankton and microzooplankton. Mesozooplankton grazing was higher on microzooplankton than on netphytoplankton [*Zhang et al.*, 1995; *Dam et al.*, 1995; Table 2]. The zooplankton equations are

$$S_3 = \lambda g_s \Lambda P_s(1 - e^{-\Lambda P_s})Z_s - g_{Zs}\Lambda Z_s(1 - e^{-\Lambda Z_s})Z_l - \mu_s Z_s - \delta_s Z_s \tag{9}$$

$$S_4 = \lambda[g_l \Lambda P_l(1 - e^{-\Lambda P_l}) + g_{Zs}\Lambda Z_s(1 - e^{-\Lambda Z_s})]Z_l - \mu_l Z_l - \delta_l Z_l \tag{10}$$

In (2), (3), (9), and (10) a modified Ivlev grazing formulation was used to account for food-acclimatized grazing and to sta-

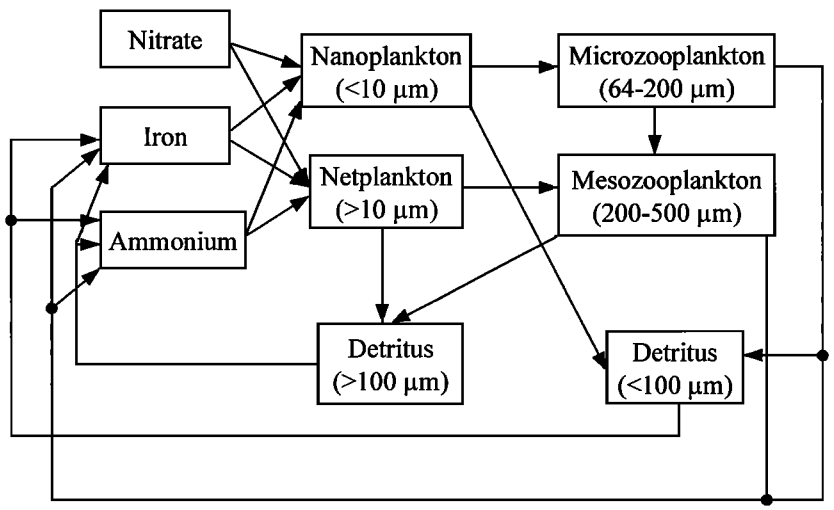

Figure 3. Flow chart of ecosystem model components. The flow chart does not include physical processes such as upwelling or sinking.

Table 2. Ecosystem Model Parameter Definitions and Values

Symbol	Value	Definition	Source
m_s	0.0	nanophytoplankton mortality, d^{-1}	
m_l	0.15	netphytoplankton mortality, d^{-1}	
G_0	0.851	phytoplankton growth rate at 0°C, d^{-1}	*Eppley* [1972]
b	0.0633	temperature coefficient for phytoplankton growth, $°C^{-1}$	*Eppley* [1972]
P^B_{max}	0.41–2.15	maximum photosynthetic rate, normalized to biomass, mg C mg C^{-1} d^{-1}	*Cullen et al.* [1992]; *Lindley et al.* [1995]
α	5280–1680	slope of the P–I curve, mg C mg C^{-1} d^{-1} $(Eins^{-2}\ s^{-1})^{-1}$	*Cullen et al.* [1992]
K_{Ns}	0.25	half-saturation constant for nitrate uptake by nanophytoplankton, mmol N m^{-3}	
K_{Nl}	0.30	half saturation constant for nitrate uptake by netphytoplankton, mmol N m^{-3}	
ψ	4.6	ammonium inhibition of nitrate, $(mmol\ N\ m^{-3})^{-1}$	*Price et al.* [1994]
K_{As}	0.05	half saturation constant for ammonium uptake by nanophytoplankton, mmol N m^{-3}	
K_{Al}	0.05	half saturation constant for ammonium uptake by netphytoplankton, mmol N m^{-3}	
K_{Fes}	34.85	half saturation constant for iron uptake by nanophytoplankton, nmol Fe m^{-3}	*Price et al.* [1994]
K_{Fel}	120.0	half saturation constant for iron uptake by netphytoplankton, nmol Fe m^{-3}	*Coale et al.* [1996a]; *Fitzwater et al.* [1996]
C:chl	58.0	phytoplankton molar carbon to chlorophyll ratio	*Eppley et al.* [1992]
γ_s	200,000	nanophytoplankton molar carbon to iron ratio	*Sunda and Huntsman* [1995]
γ_l	100,000	netphytoplankton molar carbon to iron ratio	*Sunda and Huntsman* [1995]
g_s	10.0	grazing coefficient on nanophytoplankton, d^{-1}	*Landry et al.* [1995]; *Verity et al.* [1996]
g_l	8.0	grazing coefficient on netphytoplankton, d^{-1}	*Dam et al.* [1995]; *Roman and Gauzens* [1997]
g_{Zs}	12.0	grazing coefficient on microzooplankton, d^{-1}	*Dam et al.* [1995]; *Zhang et al.* [1995]
Λ	1.	Ivlev coefficient for grazing, $(mmol\ N\ m^{-3})^{-1}$	
λ	0.75	Zooplankton assimilation efficiency (nondimensional)	
δ_s	0.1	microzooplankton death, d^{-1}	
δ_l	0.2	mesozooplankton death, d^{-1}	
μ_s	0.1	microzooplankton ammonium and iron excretion, d^{-1}	*Landry et al.* [1996]; *Hutchins et al.* [1995]
μ_l	0.1	mesozooplankton ammonium and iron excretion, d^{-1}	*Landry et al.* [1996]; *Hutchins et al.* [1995]
c_s	0.25	small detritus remineralization, d^{-1}	
c_l	0.01	large detritus remineralization, d^{-1}	

bilize the model output [*Franks et al.*, 1986]. In this formulation, the grazing rate was modulated by the Ivlev constant and the prey concentration. There were no prey thresholds for grazing in either of the zooplankton formulations, allowing a grazer to remove all prey if possible.

Along with mortality δ and recycled nutrient excretion μ, zooplankton were lost from the model domain via microzooplankton sinking and vertical migration of the mesozooplankton.

2.4.3. Detritus. Detrital packaging by larger zooplankton has been postulated as a method of removing organic carbon from the ocean surface [*Dam et al.*, 1995], so we split the detrital components into large and small size fractions with unique sinking and remineralization rates.

$$S_5 = (1 - \lambda)[g_s\Lambda P_s(1 - e^{-\Lambda P_s})Z_s + g_{Zs}\Lambda Z_s(1 - e^{-\Lambda Z_s})Z_l] + \varepsilon_s P_s + \delta_s Z_s - c_s D_s - s_s D_s + s_s D_s^{z-1} \quad (11)$$

The detrital pool was composed of dead phytoplankton and zooplankton as well as nonassimilated food from zooplankton feeding (fecal pellets). Detritus was lost from the model

$$S_6 = (1 - \lambda)[g_l\Lambda P_l(1 - e^{-\Lambda P_l})Z_l] + \varepsilon_l P_l + \delta_l Z_l - c_l D_l - s_l D_l + s_l D_l^{z-1} \quad (12)$$

domain by sinking and remineralization. Detrital sinking rates [*Diercks and Asper*, 1997; M. Roman, personal communication, 1996] exceed the numerical stability criteria for the Crank-Nicholson scheme with reasonable depth and time steps, so sinking had to be parameterized instead of explicitly modeled. Small detritus sink at 20 m d^{-1}, which was converted into a sinking loss parameter s_s of 0.667 d^{-1}. Detritus that would have been removed via sinking were subtracted at each grid point, and the amount that would have been supplied from the grid point above (D^{z-1}) was added. The same process was applied to the large detrital size fraction (sinking rate = 200 m d^{-1} and s_l = 1.67 d^{-1}).

2.4.4. Nutrients. Nitrogen was partitioned into two components, recycled nitrogen, ammonium A, and new nitrogen, nitrate N. The portion of each component taken up by phytoplankton had to be calculated for mass balance. First the total nitrate N_t and total ammonium A_t taken up by phytoplankton at a given time step were calculated:

$$N_t = \frac{N}{k_N + N} e^{-\Psi A} \qquad A_t = \frac{A}{k_A + A} \quad (13)$$

The total nitrogen taken up was then partitioned into the fractions of nitrate and ammonium consumed (new and regenerated production):

$$\pi_1 = \frac{N_t}{N_t + A_t} \qquad \pi_2 = \frac{A_t}{N_t + A_t} \quad (14)$$

Within the ecosystem model, there was only a sink for nitrate as it is taken up by phytoplankton. Phytoplankton productivity was multiplied by the fraction of total nitrogen that is nitrate to calculate this loss:

$$S_7 = -L_s\pi_1 N_{\lim s} GP_s - L_l\pi_1 N_{\lim l} GP_l \quad (15)$$

Ammonium has biological source terms from remineralized detritus and zooplankton excretion as well as losses from phy-

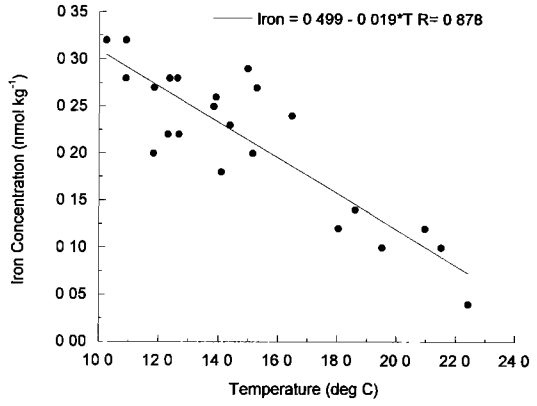

Figure 4. Iron-temperature relationship on the equator at 140°W. Samples at the limit of iron detection (0.03 nmol kg^{-1}) and outside of ±2° latitude were excluded from the calculation.

toplankton uptake. As with nitrate, the loss is calculated by using the ratio of ammonium to total nitrogen uptake:

$$S_8 = -L_s\pi_2 N_{\lim s} GP_s - L_l\pi_2 N_{\lim l} GP_l + \mu_s Z_s + \mu_l Z_l + c_s D_s + c_l D_l \quad (16)$$

The iron equation is very similar, except that we did not partition between new (i.e., externally supplied via upwelling and surface deposition) and regenerated iron. Little is known about the bio-availability of dissolved iron in the marine environment [*Wells et al.*, 1995]; therefore all the dissolved iron in the model is considered to be bioavailable, regardless of its source. Here γ_i represents the C:Fe ratio for the nanophytoplankton, netphytoplankton, and recycled iron:

$$S_9 = -\gamma_s L_s N_{\lim s} GP_s - \gamma_l L_l N_{\lim l} GP_l + \gamma_d(\mu_s Z_s + \mu_l Z_l + c_s D_s + c_d D_l) \quad (17)$$

The C:Fe ratio is difficult to measure and shows high, natural variability, with the only clear pattern consisting of a lower iron requirement for smaller phytoplankton than for larger phytoplankton [*Sunda and Huntsman*, 1995]. Therefore we chose $\gamma_s > \gamma_l$ with upper and lower limits for each parameter ($80{,}000 < \gamma_l < 150{,}000$; $150{,}000 < \gamma_s < 300{,}000$) and γ_d to be somewhere in between. All three parameters were treated as free parameters, within the given boundaries, and were adjusted to retrieve primary productivity rates that agreed with observations. The sensitivity of the model to these adjustments is addressed later in this paper.

2.5. Boundary and Initial Conditions

The upper boundary of the ecosystem model was the ocean surface, and therefore a no-flux condition for all components except iron was imposed. A constant aeolian iron flux of 10 nmol Fe m^{-3} was assumed, since there is little information regarding the temporal variability of atmospheric iron flux into the eastern Pacific [*Duce and Tindale*, 1991]. The bottom boundary was more complex. Both nitrate and iron bottom boundary conditions were functions of the daily temperature at 120 m. The temperature at this depth can be used as a proxy for the depth of the equatorial undercurrent (EUC). The amount of iron and nitrate supplied to the euphotic zone via upwelling of EUC waters is a function of the depth of the EUC, as well as the vertical velocity. For example, the EUC is deeper during El Niño and less iron is present at the base of the euphotic zone for vertical transport. The iron-temperature relationship for the model bottom boundary was determined from the FeLine and JGOFS EqPac cruise data (Figure 4), and the nitrate-temperature relationship was calculated from the JGOFS EqPac data only. The daily temperature at 120 m was retrieved from the TOGA TAO buoy at 0°N 140°W. The boundary conditions for the other components were dependent on the direction of the vertical velocity plus the sinking rate. If the total velocity was positive (upward), a no flux condition was imposed. When the total velocity was negative, the component was allowed to be advected out of the model domain.

The model was spun up with constant upwelling and light for 30 days. The resulting vertical profiles were used for the model initial conditions.

3. Results and Discussion

3.1. Five-Year Simulation

3.1.1. Physical circulation. Modeled SSTs at 140°W were affected by El Niño dynamics across the entire Pacific basin. On seasonal timescales, modeled temperature in the top 50 m at 140°W reached a maximum in mid-May, which coincided with the reversal of the westward South Equatorial Current (SEC) at this location [*McPhaden and McCarty*, 1992]. This maximum occurs almost a month later than at locations further east in the upwelling regions of the eastern equatorial Pacific (e.g., 110°W). In addition, the amplitude of the seasonal cycle in SST was smaller at 140°W than at more eastern locations. The minimum in wind speed and zonal wind velocity also occurred in mid-May; thus the maximum SST was caused by the heating of a shallower mixed layer in addition to the reduction in the advection of colder waters from below. The maximum core velocities in the EUC accompany the reversal of the SEC.

On interannual timescales, the modeled SST and its anomaly does show an ENSO dependence. However, the correlation between model SST anomaly and the Southern Oscillation Index (SOI) was only −0.5 (similar correlation is also found between Reynold's SST and SOI), indicating that there are other factors which contribute to the interannual variability at this location. One such factor may be variability in the surface wind stress. The strongest westerly wind burst of the period 1990–1994 occurred during early 1992 and extended unusually eastward of the dateline to almost 120°W (slightly stronger wind stress anomalies with a longer duration are also seen in the Special Sensor Microwave Imager data). This produces an anomalous downwelling in the model accompanied by westward currents down to 200 m (Plate 1a). It is probable that a somewhat weaker than observed model thermocline reproduces a stronger than observed response to these wind anomalies. A similar, but weaker wind-driven feature is also seen the TAO acoustic Doppler current profiler (ADCP) data, although the model produces a much stronger reversal of currents at depth. The vertical movement of the model EUC is also in qualitative agreement with the TAO data. The large negative anomaly in SST during the summer of 1992 is related to the anomalously strong easterlies during that time that leads to increased advection and upwelling and hence cooler SSTs. The model response is again stronger in accordance with the given wind forcing compared to the TAO anomalies which reach zero but do not go negative at this time.

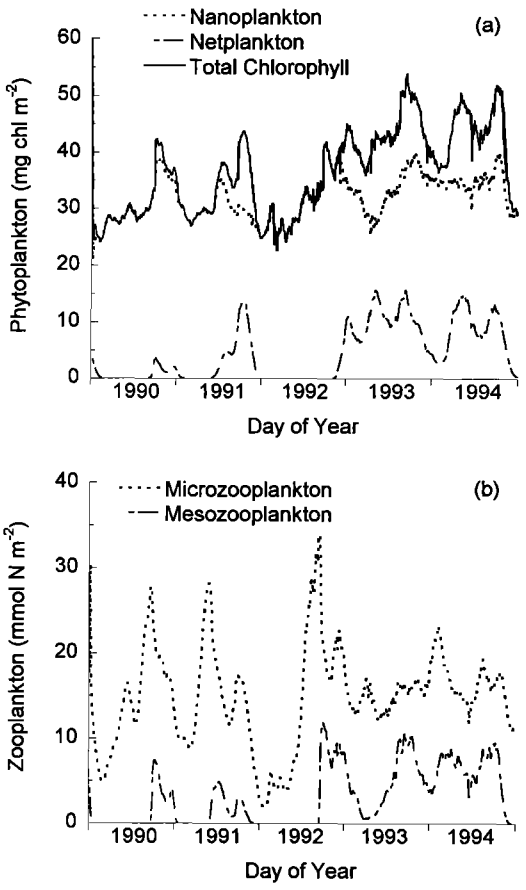

Figure 5. (a) Daily nanophytoplankton (dots), netphytoplankton (dashes), and total phytoplankton (solid), integrated to the 0.1% light level. (b) Daily microzooplankton (dots) and mesozooplankton (dashes), integrated to the 0.1% light level.

Table 3. Comparison of Ecosystem Model Output and in Situ Data

	Model Output	In situ Data
Integrated chlorophyll, 1992, mg chl m^{-2}		
Feb. 19–28	25	26[a]
March 23 to April 10	27	29[a]
Aug. 27 to Sept. 2	33	31[a]
Oct. 1–21	40	32[a]
Integrated nanophytoplankton (percent of total chlorophyll)		
Jan.–April 1992	99.9	89[b,c]
Oct.–Jan. 1992–1993	70	80[b,c]
Phytoplankton growth rates, d^{-1}		
Feb./March 1992	0.2	0.5[d,e]
Sept./Oct. 1992	0.8	0.8[d,e]
Microzooplankton removal of nanophytoplankton (percent nanophytoplankton growth)		
Feb./March 1992	95	83[f]
Sept./Oct. 1992	35	55[f]
Integrated primary productivity, mmol C m^{-2} d^{-1}		
Feb. 19–28	13	60[a]
March 23 to April 10	15	90[a]
Aug. 27 to Sept. 2	117	101[a]
Oct. 1–21	137	129[a]
New production, mmol C m^{-2} d^{-1}		
Feb./March 1992	1	4.8[g]
Sept./Oct. 1992	56	18.5[g]

[a]*Barber et al.* [1996].
[b]*Bidigare and Ondrusek* [1996].
[c]*Latasa et al.* [1997].
[d]*Murray et al.* [1994].
[e]*Verity et al.* [1996].
[f]*Landry et al.* [1995].
[g]*McCarthy et al.* [1996].

It is very difficult to assess the accuracy of model upwelling fields since no data are available for comparison. We rely on the reasonable simulation of the thermal and dynamical fields to assume that the accompanying vertical velocity fields also must be reasonable. However, as mentioned above, the anomalously strong downwelling in early 1992 is most likely a model artifact. There is a much stronger reversal of currents with depth in the model at this time, which demonstrates the model's strong response to surface wind forcing. Since the downwelling event is associated with a strong westerly wind burst in FSU winds, we can assign the blame to forcing fields. Over this short period of simulation, no clear El Niño-Southern Oscillation (ENSO) related signal can be deciphered in the model simulated or observed fields below the surface layer at 140°W.

3.1.2. Ecosystem dynamics. The vertically integrated chlorophyll time series is dominated by highs and lows following the manifestations of the 1990–1993 El Niño events (Figure 5a). Phytoplankton biomass was converted to chlorophyll using the Redfield ratio and a constant C:chl ratio of 58 [*Eppley*, 1992]. While the C:chl ratio at 0°N 140°W can vary from 20 to 200 [*Chavez et al.*, 1996], the model was more sensitive to variations in the C:Fe ratio (discussed later). Also, for ease of interpreting the model's response to changes in the C:Fe parameter, the C:chl ratio was kept constant. There was a 40% increase in the total chlorophyll from the 1991–1992 El Niño time period to the normal conditions of 1994. The chlorophyll increase was primarily due to the contribution of netphytoplankton to total chlorophyll. Integrated nanophytoplankton chlorophyll remained relatively constant during the 5-year simulation, but netphytoplankton concentrations showed more striking interannual variability. The netphytoplankton contribution to total chlorophyll ranged from 0.1 to 30% during the simulation (Figure 5a), with higher netphytoplankton chlorophyll during non El Niño time periods when there was higher iron flux to the ecosystem (Plate 2). The integrated chlorophyll output is validated by results collected during the JGOFS EqPac cruises in 1992 (Table 3) and agrees well with the data presented by *Barber et al.* [1996]. *Latasa et al.* [1997] noted a 40% increase in the total euphotic zone chlorophyll concentrations between February (El Niño) and September (La Niña) 1992. Even as total chlorophyll increased, the chlorophyll concentration in the phytoplankton <2 μm remained nearly constant, and contribution to the total chlorophyll declined from 89.5 to 80.5% [*Bidigare and Ondrusek*, 1996; *Latasa et al.*, 1997]. Despite that nanophytoplankton always dominated the phytoplankton community on the equator, there was a significant increase in diatom concentrations between the El Niño and La Niña cruises, probably due to increased iron flux to the ecosystem during La Niña [*Iriarte and Fryxell*, 1995; *Verity et al.*, 1996].

Microzooplankton showed considerably more interannual variability than their prey, the nanophytoplankton (Figure 5b). *Roman and Gauzens* [1997] found that there was higher variability of copepod (mesozooplankton) biomass during 1992 than was observed for the chlorophyll concentrations. Micro-

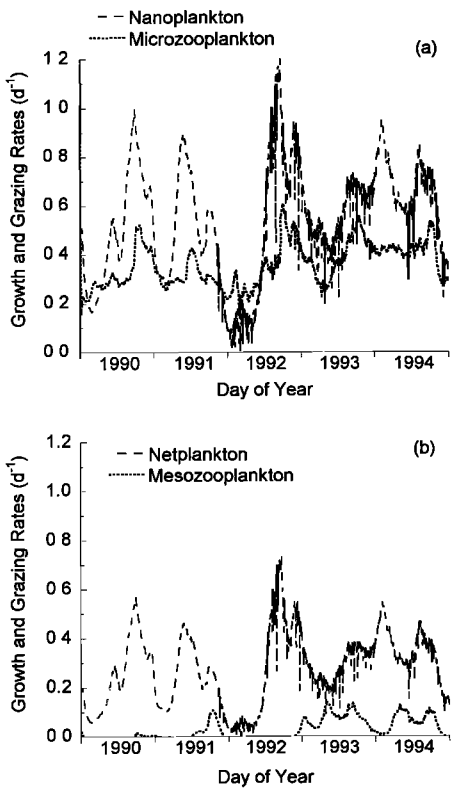

Figure 6. The 1990–1994 integrated daily phytoplankton growth and grazing removal rates (day^{-1}). Grazing removal has been multiplied by -1 for viewing ease. (a) Nanophytoplankton and microzooplankton; (b) netphytoplankton and mesozooplankton.

zooplankton biomass peaks were concurrent with the highest nanophytoplankton growth rates ($r^2 = 0.88$; Figures 5a and 6), but not always correlated with higher nanophytoplankton biomass ($r^2 = 0.31$). Peaks in the mesozooplankton biomass coincided with higher microzooplankton biomass but had the highest correlation to the microzooplankton grazing rates ($r^2 = 0.76$; Figures 5b and 6). Mesozooplankton biomass was also somewhat dependant on microphytoplankton biomass, especially during more stable conditions such as in late 1993/early 1994 (Figure 5). It appears that both food sources are necessary for the accumulation of mesozooplankton biomass. In general, there were more zooplankton following El Niño than during it, just as was found during JGOFS EqPac [*Verity et al.*, 1996; *Roman et al.*, 1995; *Zhang et al.*, 1995].

The effect of El Niño on profiles of iron and chlorophyll is also substantial (Plate 2). The combination of reduced upwelling (and downwelling) (Plate 1a), and change in the depth of the EUC as reflected in the temperature profiles (Plate 1b) reduces the vertical iron flux to the euphotic zone. There was a seasonal signal of higher iron flux in the fall than in the spring, but the interannual El Niño signature dominated the iron profiles. The interannual variability was also reflected in the chlorophyll profiles (Plate 2b). The formation of a deep chlorophyll maximum (DCM) did not occur during El Niño events because the downwelling signal disrupted the stability of the area just below the mixed layer, where the DCM usually formed. Also, the iron concentrations at depth were too low to support phytoplankton growth in the region of prior DCMs. The lack of a DCM during the El Niño portion of the EqPac program was noted by both *Bidigare and Ondrusek* [1996] and *Barber et al.* [1996]. The magnitude of the DCM was also affected by El Niño, with higher chlorophyll concentrations in the DCM during 1993–1994 than in the earlier years.

The two phytoplankton size fractions had different DCM depths (Plate 3). There were always more nanophytoplankton present than netphytoplankton, and the nanophytoplankton DCM was shallower. Previous models have also shown different depth profiles for different phytoplankton size fractions, such as the deeper DCM for larger phytoplankton in *Moisan and Hofmann*'s [1996] model of the California coastal current system. The different DCM depths in that case were due to different spectral photosynthetic parameters for each phytoplankton species in their model, whereas the different size fractions in our model have the same photosynthetic parameters. Instead, the DCM for each size fraction was found at the depth of the iron isopleth that corresponds to that size fraction's half-saturation constant for iron uptake. Since the depth of the half-saturation constant for nanophytoplankton (35 nmol Fe m^{-3}) was shallower than the netphytoplankton's (120 nmol Fe m^{-3}), the nanophytoplankton DCM was shallower than the netphytoplankton DCM (Plate 2a and 3). In addition, netphytoplankton had a higher sinking rate than nanophytoplankton, which would aid in the separation of the two size fractions with depth. Finally, mesozooplankton migration could have imposed more grazing pressure on shallower netphytoplankton, since most of the mesozooplankton were found in the upper water column (data not shown) and allowed for more netphytoplankton accumulation at depth.

In addition to interannual variability in phytoplankton imposed by El Niño, there was also a seasonal signal. Profiles of monthly averaged chlorophyll show that the DCM was much more prominent during the latter half of the year (Figure 7). There are no field data from the region with sufficient temporal scale to resolve this seasonal signal, but data collected during JGOFS EqPac did show a more prominent DCM in October than in February 1992 [*Bidigare and Ondrusek*, 1996; *Barber et al.*, 1996; *Landry et al.*, 1996]. *Peña et al.* [1992] also found a prominent DCM at 135°W on the equator in April 1988, while *Cullen et al.* [1992] recorded a small DCM at 150°W in February–March 1988. The field data from different years and locations are difficult to reconcile, but our results suggest that there is indeed seasonal variability at this location.

Vertical advection appears to be the driving force behind the iron flux to the euphotic zone and the model interannual variability. *Coale et al.* [1996a] calculated that 85–95% of the iron flux to the euphotic zone at 0°N 140°W was from upwelling of subsurface iron, and we calculated a similar range of 80–99%. One model simulation was run with no vertical advection ($w = 0$) and there was little, if any, interannual variability in the iron, phytoplankton, and zooplankton components (Plate 4). Iron concentration at the bottom boundary still showed interannual variability because of its relationship with temperature and the EUC (Plate 4a), but diffusion was too small to transport sufficient iron to the euphotic zone to support as much phytoplankton as in the full advection simulation (Plate 2). There was a constant DCM at ~80 m, with a chlorophyll minimum at ~20 m depth (Plate 4b). Chlorophyll was elevated at the surface due to aeolian iron flux and at depth due to diffusion of iron from the bottom boundary.

Modeled integrated daily phytoplankton growth rates agreed well with observations since the Fe:chl ratio was adjusted to achieve this result. Average growth rates over the

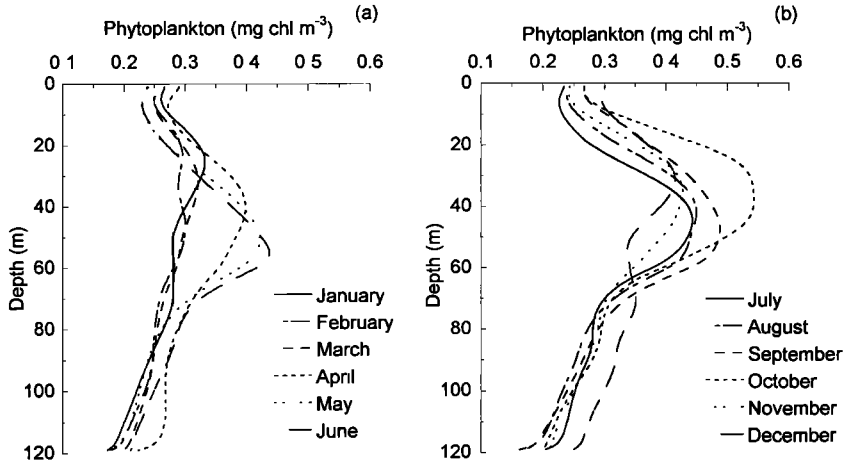

Figure 7. (a) Spring and (b) fall 5-year monthly average phytoplankton (mg chl m^{-3}) profiles. January (solid); February (dot dash); March (dash); April (short dash); May (dots); June (long dash); July (solid); August (dot dash); September (dash); October (short dash); November (dots); December (long dash).

water column were 0.5 d^{-1} in February/March and 0.8 d^{-1} in September/October [*Murray et al.*, 1994; *Verity et al.*, 1996] as compared to our modeled growth rates of 0.2 and 0.8 for the same time periods (Figure 6; Table 3). Nanophytoplankton mortality due to microzooplankton grazing mirrored nanophytoplankton growth, as reported by *Landry et al.* [1995]. *Verity et al.* [1996] estimated that microzooplankton grazing removed up to 133% of the phytoplankton growth each day, which is higher than our model estimate. Microzooplankton removal of nanophytoplankton in our model ranged from 35 to 95% and was closer to the Landry et al. estimates of 55 to 83% removal of nanophytoplankton growth by the microzooplankton. The higher removal percentage occurred during El Niño, both in the field and in our model. In contrast, mesozooplankton removal rates do not mirror netphytoplankton growth rates (Figure 6b); yet grazing is probably responsible for regulating netphytoplankton biomass during more stable conditions such as during late 1993. *Dam et al.* [1995] found that mesozooplankton only removed ~1–9% of the total chlorophyll during 1992, which may have been all the netphytoplankton [*Bidigare and Ondrusek*, 1997]. Dam et al. and *Zhang et al.* [1995] calculated that the mesozooplankton must ingest microzooplankton and detritus to satisfy their daily carbon requirements. The model output reflects this in that only ~30% of the nitrogen ingested by mesozooplankton is derived from phytoplankton, with most of that supplied from the netphytoplankton size fraction.

One discrepancy between the model output and the JGOFS data was in growth and primary productivity rates during early 1992 (Table 3). Average phytoplankton growth rates during early 1992 were much lower than measured rates (0.15 d^{-1} as compared to 0.53 d^{-1}) [*Murray et al.*, 1994]. Integrated net primary production (Figure 8) agreed well with *Barber et al.* [1996] during late 1992 but was much lower during El Niño (Table 3). Lower productivity was expected during El Niño because of reduced iron flux, changes in the ecosystem structure, and more cloud cover that led to a reduction in the surface PAR during early 1992, but the model output was much lower than in situ data. Along with decreased iron flux in early 1992, downwelling in the middle of the water column (Plate 1a) during the same time period removed phytoplankton from the euphotic zone. As described earlier, the physical model output for this period is suspect, and the advection was most likely too strong and negative. The anomalous downwelling is probably the main reason for much lower than observed growth and primary production rates during the El Niño period of 1992.

The modeled plankton biomass follows the expected patterns over most of the 5-year period, with less chlorophyll in general and less netphytoplankton specifically during El Niño events, but the interrelationships between the components can be complex. For example, the netphytoplankton populations are lower than the observed JGOFS EqPac data set in the fall of 1992 but eventually reach EqPac levels by early 1993 (Figure 5). The netphytoplankton populations crashed during the 1992 El Niño in the model, as a result of the downwelling in the physical model. This population crash led to a slower than observed increase in the netphytoplankton biomass in the second half of 1992, even though their growth rates were quite high at this time (Figure 6). In addition, it appears that nanophytoplankton chlorophyll actually decreases in mid-1993 while netphytoplankton chlorophyll is still increasing. The nanophytoplankton decrease is either a result of predator-predator-prey interactions between the zooplankton and the nanophytoplankton or the nanophytoplankton concentration could be approaching its steady state equilibrium value [*Leonard*, 1998] as the iron concentrations did not undergo very large oscillations in 1993 (Plate 2).

The phrase "new production" is generally reserved to describe the amount of new nitrogen (nitrate in this region) taken up by phytoplankton. The f ratio denotes the fraction of total production that is new, as opposed to regenerated or ammonium based. The f ratios in the central Pacific averaged ~0.17 in 1992, with little variation between El Niño and normal conditions [*McCarthy et al.*, 1996]. Since the primary production in our model is iron limited, a traditional f ratio is probably an inadequate measure of new versus recycled productivity for this simulation. Instead we used a ratio of the amount of iron taken up at each time step to the amount of iron recycled at each time step. This "new iron" ratio shows significant variability, with a low of nearly 0 during the times of lowest iron flux and a high of 0.6 during more normal conditions (Figure 9). Iron-based new production ranges from 1 to 56 mmol C m^{-2} d^{-1} (Table 3). The iron-based new production and f ratio are higher than the traditional nitrate measurements, because

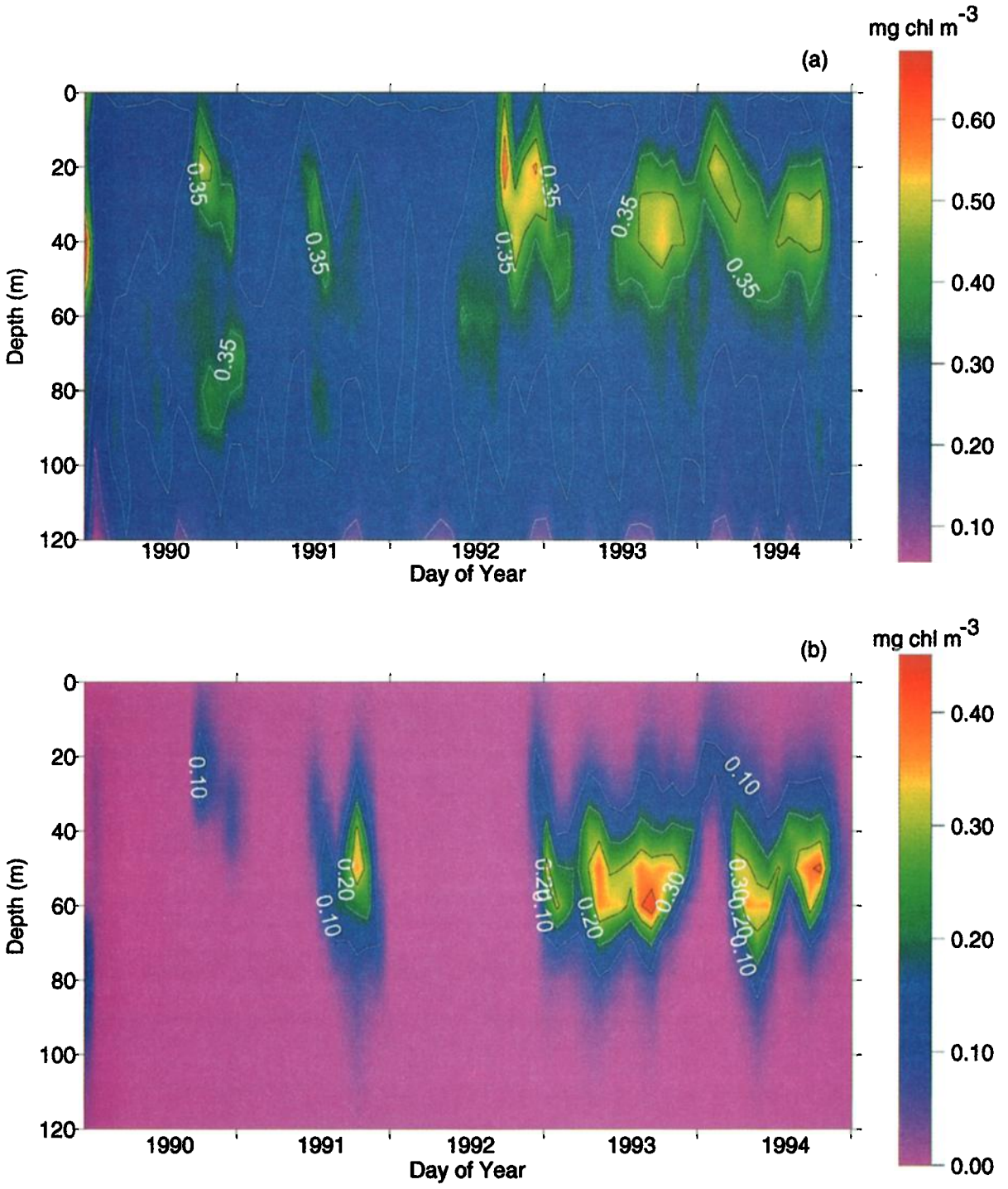

Plate 3. Modeled daily (a) nanophytoplankton and (b) netphytoplankton from 1990 to 1994. Contour intervals are 0.1 mg chl m^{-3}.

nitrate uptake at 0°N 140°W is suppressed due to iron limitation and ammonium inhibition [*Price et al.*, 1994]. In oceanic regions where nitrate is not necessarily the limiting nutrient, traditional f ratios may be too low and the supply and regeneration of the limiting nutrient should be taken into consideration.

One caveat to this approach is the difference between nitrogen and iron utilization by phytoplankton. Recycled nitrogen in the form of ammonium is preferentially taken up by phytoplankton over nitrate [*Price et al.*, 1994]. New and recycled iron in this model have no such distinction. In addition, the bioavailability of recycled iron may be quite different from that of newly supplied dissolved iron [*Wells et al.*, 1995]. Unfortunately, determining when and how dissolved iron becomes available to phytoplankton is not trivial and little is known about phytoplankton preferences for new versus recycled iron. If phytoplankton do have a strong preference for one form of iron, as they do for nitrogen, our new production estimates

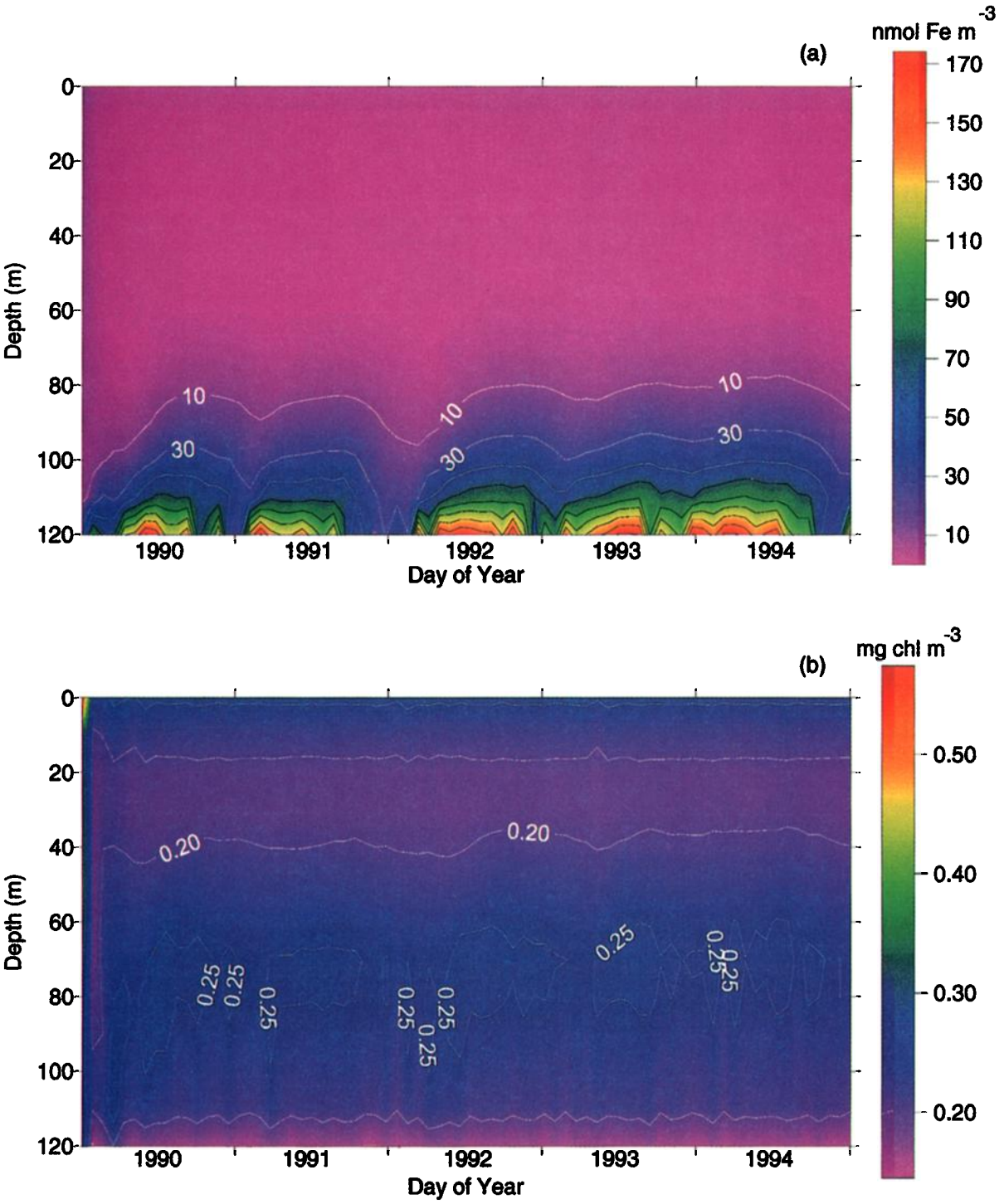

Plate 4. Modeled profiles of (a) iron and (b) phytoplankton from 1990 to 1994 with $w = 0$. Iron contours are 20 nmol Fe m^{-3}, and phytoplankton contours are 0.05 mg chl m^{-3}.

could be severe over- or underestimations of the export production in iron-limited regions. Yet these calculations are interesting if only to bring attention to the possible errors in calculating new production if the focus is inadvertently on the nonlimiting nutrient.

A consistent observation of oceanic ecosystems is that oligotrophic open ocean regions are dominated by small phytoplankton while large phytoplankton dominate highly productive and nutrient rich coastal areas [*Malone*, 1971]. This observation has been linked to the reasoning that large cells depend mainly on nitrate for growth and small cells use regenerated nitrogen (ammonia) for growth [*Parsons and Takahashi*, 1973; *Malone*, 1980]. An additional explanation is that small cells have higher surface-to-volume ratios and the ability to sustain higher growth rates at lower nitrogen concentrations than larger cells [*Chisholm*, 1992]. The ecosystem dynamics in

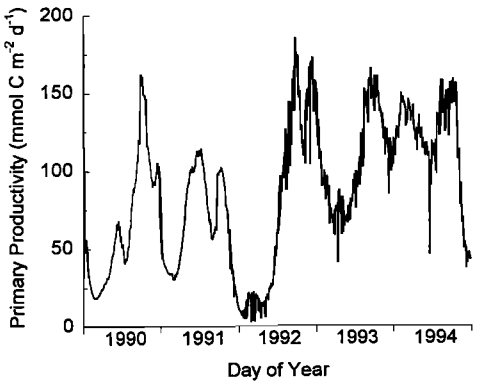

Figure 8. The 1990–1994 modeled daily primary production, integrated to the 0.1% light level.

the equatorial Pacific demonstrate that it is not even necessarily the nutrient that is important but that larger cells depend on new nutrients and/or higher nutrient flux whereas smaller cells can be maintained on recycled nutrients only. When the modeled ecosystem was composed of almost all nanophytoplankton, primary production was lower, as was the new iron flux to the ecosystem. As the iron flux increased, so did the netphytoplankton, primary productivity, and new production. *Landry et al.* [1997] came to the conclusion that the equatorial Pacific ecosystem is essentially the same as the central gyres, except that it is iron limited rather than nitrate limited. On the basis of our model results we would argue that in this ecosystem small phytoplankton are supported by recycled production and large phytoplankton are supported by new production.

3.2. Sensitivity Analysis

The ecosystem model was tested for both stability and sensitivity to various parameters. The stability analysis demonstrated that the unforced ecosystem model always returned to the equilibrium solution, regardless of initial conditions or perturbations within the model run [*Leonard*, 1998]. The stability analysis methods and results are thoroughly covered in another paper, so this section will concentrate on the model's sensitivity to various biological parameters. The analysis will focus on those parameters that control the flow of iron through the food web and includes zooplankton grazing, phytoplankton and zooplankton mortality, detrital sinking rates, detrital recycling rates, and the phytoplankton C:Fe ratio. The model was run for 1 year, 1990, with one parameter changed in turn. For model output, each component was vertically integrated. Then the yearly average was calculated, and the percent difference from the standard run was used to establish the model's sensitivity to a given parameter.

The ecosystem model output was not very sensitive to detrital sinking and regeneration rates (Table 4). The only component significantly affected by changes in these parameters was the netphytoplankton biomass. In addition, vertical chlorophyll profiles, as noted by the depth of the deep chlorophyll maximum, were not particularly sensitive to any of the tested parameters.

The model was most sensitive to the phytoplankton and zooplankton closure terms (Table 4). The greatest changes in integrated nanophytoplankton biomass came from reduction of the microzooplankton grazing rate and the increase in nanophytoplankton mortality. Primary productivity was also responsive to closure terms on the phytoplankton with negative percent differences due to increased phytoplankton death and a large positive difference when microzooplankton grazing was relaxed. Grazing rates for this ecosystem are relatively well known [*Landry et al.*, 1995; *Dam et al.*, 1995; *Verity et al.*, 1996; *Roman and Gauzens*, 1998], but phytoplankton and zooplankton mortality rates are not. Most ecosystem models are very sensitive to mortality terms [e.g., *Steele and Henderson*, 1995], but since little is known about natural mortality rates, they are usually used as free parameters to adjust the model output to observed values, as was done in this case.

Decreasing the nanophytoplankton C:Fe ratio decreased primary productivity by 22%, as well as reducing the netphytoplankton biomass by 68% (Table 4). Primary productivity had a higher response to changes in this parameter than did the nanophytoplankton biomass, which only decrease by 4% in the same simulation. These percentages suggest that while phytoplankton biomass does affect average primary productivity, results from this model are very dependent upon the C:Fe molar ratio selected. The C:Fe ratio for phytoplankton is quite variable, ranging from 0.1 to 2 μmol:mol [*Sunda et al.*, 1991]. Again, little is known about the actual C:Fe ratio for phytoplankton in the equatorial Pacific, other than oceanic phytoplankton have a lower iron requirement for growth than coastal species [*Sunda and Huntsman*, 1995]. *Wells et al.* [1995] advocate the collection of more intracellular C:Fe ratios, as do we, to further the understanding of iron's role in phytoplankton growth and production. For this study we were forced to use the iron ratio as a free parameter (within upper and lower limits) to adjust the primary production and phytoplankton size fraction distribution to observed levels.

Netphytoplankton concentrations were sensitive to almost all parameter modifications (Table 4). As noted by both *Leonard* [1998] and *Barbeau et al.* [1996] netphytoplankton growth was dependent on microzooplankton grazing of nanophytoplankton. Nanophytoplankton must be removed from the ecosystem via either grazing or mortality in order for the iron flux to support two size fractions of phytoplankton, as can be seen in the netphytoplankton response to an increase in the nanophytoplankton mortality rate (Table 4). In addition, netphytoplankton are more sensitive to the nonlinear interactions between the model components. A change in any component that affected the amount of iron available for uptake was manifest in the netphytoplankton concentration. Most parameter modifications that significantly increased or decreased nanophytoplankton had the opposite effect on netphytoplankton. Also, small changes in iron supply, such as detrital recycling rates,

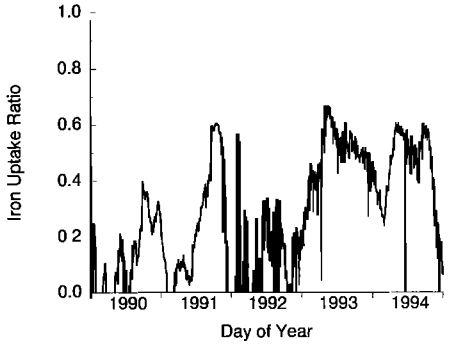

Figure 9. The 1990–1994 ratio of total iron uptake to new iron supplied via upwelling.

Table 4. Results of Sensitivity Analysis

Parameter	Parameter Range	Nanophytoplankton	Netphytoplankton	DCM	Primary Productivity
Microzooplankton grazing, g_s	5	51	−90	−5.8	21
	15	−21	103	4.3	−10
Macrozooplankton grazing, g_l	4	−1.3	43	1.2	−2.2
	12	0.6	−21	−1.2	1.1
Macrozooplankton grazing, g_{Zs}	6	−5.3	101	4.2	−5.8
	18	7.2	−47	−9.7	6.7
Nanophytoplankton death, m_s	0.1	−40	186	8.9	−10
Netphytoplankton death, m_l	0.05	−0.8	618	−3.9	−16
	0.25	0.8	−96	−1.9	4.4
Microzooplankton death, δ_s	0.	−16	−34	−21	−3.3
	0.2	16	17	−9.5	1.9
Macrozooplankton death, δ_l	0.1	−1.4	−31	−5.2	5.6
	0.3	4.1	38	1.6	−3.1
Small detritus recycling, c_s	0.15	−0.3	−22	−1.9	−5.3
	0.35	0.2	8.4	1.4	2.6
Large detritus recycling, c_l	0.	−0.3	−22	−1.9	−5.4
	0.05	−0.3	−21	−1.9	−5.2
Small detritus sinking, s_s	10	−0.1	−7.2	−0.7	−1.7
	30	−0.7	−31	−2.3	−7.4
Large detritus sinking, s_l	150	1.3	−22	−1.9	−5.3
	250	−0.7	−22	−1.9	−5.3
Nanophytoplankton C:Fe, γ_s	150,000	−4.4	−68	4.8	−22
	250,000	1.8	11	−0.7	8.2
Netphytoplankton C:Fe, γ_l	50,000	−2.7	−34	−1.3	−12
	150,000	−0.2	−17	−2.3	−1.8

DCM, deep chlorophyll maximum. Values are the percent change in the average yearly integrated component from the base run. Top numbers indicate beginning of range; bottom numbers indicate end of range.

had a large effect on netphytoplankton populations. However, changes in netphytoplankton biomass did not directly impact primary production. Primary productivity was more dependent on nanophytoplankton growth than netphytoplankton, since nanophytoplankton had consistently higher growth rates than netphytoplankton (Figure 6).

4. Summary and Conclusions

The effect of El Niño on the iron supply and ecosystem at 0°N 140°W was investigated using a one-dimensional, nine-component ecosystem model. This model was forced with vertical advection from an ocean GCM [*Murtugudde and Busalacchi*, 1998], vertical eddy diffusivity calculated from in situ data, and modeled atmospheric irradiance [*Gregg and Carder*, 1990]. Ecosystem variability was dominated by the 1990–1992 El Niño event. While nanophytoplankton concentrations remained relatively constant over the 5-year simulation, netphytoplankton concentrations decreased substantially during El Niño time periods. Microzooplankton grazing constrained nanophytoplankton biomass and mesozooplankton grazing was unrelated to netphytoplankton growth rates. Primary production also showed considerable interannual variability, with up to 50% more production during normal conditions. Theoretical calculations of iron-based new production were 3 times higher than measured nitrate-based new production estimates. While the iron-based calculations may be high, the concept of the "limiting nutrient" when making new production estimates should be taken into consideration.

The model output supports the hypothesis that equatorial Pacific phytoplankton are both iron-limited and grazer-controlled. The model also successfully reproduces much of the data collected and the general ecosystem composition patterns observed during the 1992 JGOFS EqPac field program. Iron supply determines what phytoplankton size fraction will be most prominent, while grazing pressure keeps the population below the system's carrying capacity for smaller phytoplankton. El Niño events not only modify general chlorophyll concentrations and primary production totals but change the entire ecosystem composition. The ecosystem goes from one steady state with a population of larger phytoplankton and relatively high levels of new production, to a recycled-nutrient based system dominated by small phytoplankton and zooplankton. Future plans for this model include incorporation into the three-dimensional GCM of *Murtugudde and Busalacchi* [1998]. The three-dimensional model should test the switching mechanism between iron- and nitrate-limited ecosystems in the eastern and western Pacific, as well as providing insight as how an El Niño affects primary production across the entire Pacific Basin.

Acknowledgments. The authors would like to thank the U.S. JGOFS and TOGA-TAO programs for use of their extensive data sets. The authors would also like to thank J. Christian, W. Boicourt, J. Carton, and two anonymous reviewers for comments that greatly improved this manuscript. Financial support for this work was provided by the NASA Graduate Student Researcher Program (C.L.L.) and the NASA Ocean Biogeochemistry Program (C.R.M.). This work was done by C.L.L. in partial fulfillment of the requirements for a Ph.D. at the University of Maryland.

References

Barbeau, K., J. W. Moffett, D. A. Caron, P. L. Croot, and D. L. Erdner, Role of protozoan grazing in relieving iron limitation of phytoplankton, *Nature*, *380*, 61–64, 1996.

Barber, R. T., and F. P. Chavez, Ocean variability in relation to living resources during the 1982–83 El Niño, *Nature*, *319*, 279–285, 1986.

Barber, R. T., M. P. Sanderson, S. T. Lindley, F. Chai, J. Newton, C. C. Trees, D. G. Foley, and F. P. Chavez, Primary productivity and its

regulation in the equatorial Pacific during and following the 1991–92 El Niño, *Deep Sea Res. Part II, 43*, 933–969, 1996.

Behrenfeld, M. J., and P. G. Falkowski, Photosynthetic rates derived from satellite-based chlorophyll concentration, *Limnol. Oceanogr., 42*, 1–20, 1997.

Berger, W. H., Global maps of ocean productivity, in *Productivity of the Ocean: Present and Past*, edited by W. H. Berger, V. S. Smetacek, and G. Wefer, pp. 429–455, John Wiley, New York, 1989.

Bidigare, R. R., and M. E. Ondrusek, Spatial and temporal variability of phytoplankton pigment distributions in the central equatorial Pacific Ocean, *Deep Sea Res. Part II, 43*, 809–833, 1996.

Chai, F., S. T. Lindley, and R. T. Barber, Origin and maintenance of a high nitrate condition in the equatorial Pacific, *Deep Sea Res. Part II, 43*, 1031–1064, 1996.

Chavez, F. P., K. R. Buck, S. K. Service, J. Newton, and R. T. Barber, Phytoplankton variability in the eastern and central tropical Pacific, *Deep Sea Res. Part II, 43*, 810–835, 1996.

Chen, D., A. Busalacchi, and L. Rothstein, The roles of vertical mixing, solar radiation, and wind stress in a model simulation of the sea surface temperature seasonal cycle in the tropical Pacific Ocean, *J. Geophys. Res., 99*, 20,345–20,359, 1994.

Chisholm, S. W., Phytoplankton size, in *Primary Productivity and Biogeochemical Cycles in the Sea*, edited by P. G. Falkowski and A. D. Woodhead, pp. 213–237, Plenum, New York, 1992.

Coale, K. H., S. E. Fitzwater, R. M. Gordon, K. S. Johnson, and R. T. Barber, Control of community growth and export production by upwelled iron in the equatorial Pacific Ocean, *Nature, 379*, 621–624, 1996a.

Coale, K. H. et al., A massive phytoplankton bloom induced by an ecosystem-scale iron fertilization experiment in the equatorial Pacific Ocean, *Nature, 383*, 495–501, 1996b.

Cullen, J. J., M. R. Lewis, C. O. Davis, and R. T. Barber, Photosynthetic characteristics and estimated growth rates indicate grazing is the proximate control of primary production in the equatorial Pacific, *J. Geophys. Res., 97*, 639–654, 1992.

Dam, H. G., X. Zhang, M. Butler, and M. R. Roman, Mesozooplankton grazing and metabolism at the equator in the central Pacific: Implications for carbon and nitrogen fluxes, *Deep Sea Res. Part II, 42*, 735–756, 1995.

Diercks, A.-R., and V. L. Asper, *In situ* settling speeds of marine snow aggregates below the mixed layer: Black Sea and Gulf of Mexico, *Deep Sea Res Part II, 44*, 385–398, 1997.

Duce, R. A., and N. W. Tindale, Atmospheric transport of iron and its deposition in the ocean, *Limnol. Oceanogr., 36*, 1715–1726, 1991.

Eppley, R. W., Temperature and phytoplankton growth in the sea, *Fish. Bull., 70*, 1063–1085, 1972.

Eppley, R. W., Standing stocks of particulate carbon and nitrogen in the equatorial Pacific at 150°W, *J. Geophys. Res., 97*, 655–661, 1992.

Fitzwater, S. E., K. H. Coale, R. M. Gordon, K. S. Johnson, and M. E. Ondrusek, Iron deficiency and phytoplankton growth in the equatorial Pacific, *Deep Sea Res. Part II, 43*, 995–1015, 1996.

Frank, P. J. S., J. S. Wroblewski, and G. R. Flierl, Behavior of a simple plankton model with food-level acclimation by herbivores, *Mar. Biol., 91*, 121–129, 1986.

Frouin, R., D. W. Lingner, C. Gautier, K. S. Baker, and R. C. Smith, A simple analytical formula to compute clear sky total and photosynthetically available solar irradiance at the ocean surface, *J. Geophys. Res., 94*, 9731–9742, 1989.

Gent, P., and M. A. Cane, A reduced gravity, primitive equation model of the upper equatorial ocean, *J. Comput. Phys., 81*, 444–480, 1990.

Gregg, W. W., and K. L. Carder, A simple spectral solar irradiance model for cloudless maritime atmospheres, *Limnol. Oceanogr., 35*, 1657–1675, 1990.

Hutchins, D. A., W. X. Wang, and N. S. Fisher, Copepod grazing and the biogeochemical fate of diatom iron, *Limnol. Oceanogr., 40*, 989–994, 1995.

Iriarte, J. L., and G. A. Fryxell, Micro-phytoplankton of the equatorial Pacific (140°W) during the JGOFS EqPac Time Series studies: March to April and October 1992, *Deep Sea Res. Part II, 42*, 559–584, 1995.

Landry, M. R., J. Constantinou, and J. Kirshtein, Microzooplankton grazing in the central equatorial Pacific during February and August, 1992, *Deep Sea Res. Part II, 42*, 657–671, 1995.

Landry, M. R., J. Kirshtein, and J. Constantinou, Abundances and distributions of picoplankton populations in the central equatorial Pacific from 12°N to 12°S, 140°W, *Deep Sea Res. Part II, 43*, 871–890, 1996.

Landry, M. R., et al., Iron and grazing constraints on primary production in the central equatorial Pacific: An EqPac synthesis, *Limnol. Oceanogr., 42*, 405–418, 1997.

Latasa, M., M. R. Landry, L. Schluter, and R. R. Bidigare, Pigment-specific growth and grazing rates of phytoplankton in the central equatorial Pacific, *Limnol. Oceanogr., 42*, 289–298, 1997.

Leonard, C. L., El Niño, iron, and the central equatorial Pacific ecosystem: A modeling study, Ph.D. dissertation, 141 pp., Univ. of Md., College Park, 1998.

Leonard, C. L., and C. R. McClain, Assessment of interannual variation (1979–1986) in pigment concentrations in the tropical Pacific using the CZCS, *Int. J. Remote Sens., 17*, 721–732, 1996.

Lindley, S. T., R. R. Bidigare, and R. T. Barber, Phytoplankton photosynthesis parameters along 140°W in the equatorial Pacific, *Deep Sea Res. Part II, 42*, 441–464, 1995.

Loukos, H., B. Frost, D. E. Harrison, and J. W. Murray, An ecosystem model with iron limitation of primary productivity in the equatorial Pacific at 140°W, *Deep Sea Res. Part II, 44*, 2221–2249, 1997.

Malone, T. C., The relative importance of nanoplankton and netplankton as primary producers in tropical and neritic phytoplankton communities, *Limnol. Oceanogr., 16*, 633–639, 1971.

Malone, T. C., Algal size, in *The Physiological Ecology of Phytoplankton*, edited by I. Morris, pp. 433–463, Blackwell, Cambridge, Mass., 1980.

Martin, J. H., R. M. Gordon, and S. E. Fitzwater, The case for iron, *Limnol. Oceanogr., 36*, 1793–1800, 1991.

Martin, J. H., et al., Testing the iron hypothesis in ecosystems of the equatorial Pacific Ocean, *Nature, 371*, 123–129, 1994.

McCarthy, J. J., C. Garside, J. L. Nevins, and R. T. Barber, New production along 140°W in the equatorial Pacific during and following the 1992 El Niño event, *Deep Sea Res. Part II, 43*, 1065–1093, 1996.

McPhaden, M., and M. McCarty, Mean seasonal cycles and interannual variations at 0°, 110°W and 0°, 140°W during 1980–1991, *NOAA Tech. Memo. ERL PMEL-95*, pp. 67–118, Seattle, Wash., 1992.

Moisan, J. R., and E. E. Hofmann, Modeling nutrient and plankton processes in the California coastal transition zone, 1, A time- and depth-dependent model, *J. Geophys. Res., 101*, 22,647–22,676, 1996.

Morel, A., Optical modeling of the upper ocean in relation to its biogenous matter content (Case 1 waters), *J. Geophys. Res., 93*, 10,749–10,768, 1988.

Murray, J. W., R. T. Barber, M. R. Roman, M. P. Bacon, and R. A. Feely, Physical and biological controls on carbon cycling in the equatorial Pacific, *Science, 266*, 58–65, 1994.

Murtugudde, R., and A. J. Busalacchi, Salinity effects in a tropical ocean model, *J. Geophys. Res., 103*, 3283–3300, 1998.

Murtugudde, R., R. Seager, and A. Busalacchi, Simulation of the tropical oceans with an ocean GCM coupled to an atmospheric mixed layer model, *J. Clim., 9*, 1795–1815, 1996.

Pacanowski, R. C., and S. G. H. Philander, Parameterization of vertical mixing in numerical models of tropical oceans, *J. Phys. Oceanogr., 11*, 1443–1451, 1981.

Parsons, T. R., and M. Takahashi, Environmental control of phytoplankton size, *Limnol. Oceanogr., 18*, 511–515, 1973.

Peña, M. A., M. R. Lewis, and W. G. Harrison, Primary productivity and size structure of phytoplankton biomass on a transect of the equator at 135°W in the Pacific Ocean, *Deep Sea Res. Part II, 37*, 295–315, 1992.

Price, N. M., B. A. Ahner, and F. M. M. Morel, The equatorial Pacific Ocean: Grazer-controlled phytoplankton populations in an iron-limited ecosystem, *Limnol. Oceanogr., 39*, 520–534, 1994.

Roman, M. R., and A. L. Gauzens, Copepod grazing in the equatorial Pacific, *Limnol. Oceanogr., 42*, 623–634. 1997.

Roman, M. R., H. G. Dam, A. L. Gauzens, J. Urban-Rich, D. G. Foley, and T. D. Dickey, Zooplankton variability on the equator at 140°W during the JGOFS EqPac study, *Deep Sea Res. Part II, 42*, 673–694, 1995.

Steele, J. H., and E. W. Henderson, Predation control of plankton demography, *ICES J. Mar. Sci., 52*, 565–573, 1995.

Sunda, W. G., and S. A. Hunstman, Iron uptake and growth limitation in oceanic and coastal phytoplankton, *Mar. Chem., 50*, 189–206, 1995.

Sunda, W. G., D. G. Swift, and S. A. Huntsman, Low iron requirement for growth in oceanic phytoplankton, *Nature, 351*, 55–57, 1991.

Tai, K.-S., and C. R. McClain, IDAPAK: Interactive analysis of oceanographic and meteorological data for UNIX workstations, paper presented at 12th International Conference on Interactive Information and Processing Systems for Meteorology, Oceanography, and Hydrology, Am. Meteorol. Soc., Atlanta, Ga., 1996.

Verity, P. G., D. K. Stoecker, M. E. Sierack, and J. R. Nelson, Microzooplankton grazing of primary production at 140°W in the equatorial Pacific, *Deep Sea Res. Part II*, *43*, 1227–1255, 1996.

Wells, M. L., N. M. Price, and K. W. Bruland, Iron chemistry in seawater and its relationship to phytoplankton: A workshop report, *Mar. Chem.*, *48*, 157–182, 1995.

Zhang, X., H. G. Dam, J. R. White, and M. R. Roman, Latitudinal variations in mesozooplankton grazing in the central tropical Pacific during the U.S. JGOFS EqPac study, *Deep Sea Res. Part II*, *42*, 695–714, 1995.

L. W. Harding, Maryland Sea Grant College, University of Maryland, College Park, MD 20742. (larry@kestrel.umd.edu)

E. E. Hofmann, Center for Physical Coastal Oceanography, Old Dominion University, Norfolk, VA 23529. (hofmann@cepo.odu.edu)

C. L. Leonard, Joint Institute for Marine and Atmospheric Research, 1000 Pope Road, University of Hawaii, Honolulu, HI 96822. (carrie@soest.hawaii.edu)

C. R. McClain, SeaWiFS Project Office, NASA Goddard Space Flight Center, Greenbelt, MD 20771. (mcclain@calval.gsfc.nasa.gov)

R. Murtugudde, Joint Center for Earth Systems Science, University of Maryland, College Park, MD 20742. (ragu@seetha.gsfc.nasa.gov)

(Received April 7, 1998; revised September 18, 1998;
accepted October 9, 1998.)